OPTICS

# Coherent light control of a metastable hidden state

**Julian Maklar[1], Jit Sarkar[1], Shuo Dong[1], Yaroslav A. Gerasimenko[2,3]†, Tommaso Pincelli[1], Samuel Beaulieu[1]‡, Patrick S. Kirchmann[4], Jonathan A. Sobota[4], Shuolong Yang[4,5]§, Dominik Leuenberger[4,5], Robert G. Moore[4]||, Zhi-Xun Shen[4,5], Martin Wolf[1], Dragan Mihailovic[2,3], Ralph Ernstorfer[1,6], Laurenz Rettig[1]***



**Metastable phases present a promising route to expand the functionality of complex materials. Of particular interest are light-induced metastable phases that are inaccessible under equilibrium conditions, as they often host new, emergent properties switchable on ultrafast timescales. However, the processes governing the trajectories to such hidden phases remain largely unexplored. Here, using time- and angle-resolved photoemission spectroscopy, we investigate the ultrafast dynamics of the formation of a hidden quantum state in the layered dichalcogenide 1*T*-$TaS_2$ upon photoexcitation. Our results reveal the nonthermal character of the transition governed by a collective charge-density-wave excitation. Using a double-pulse excitation of the structural mode, we show vibrational coherent control of the phase-transition efficiency. Our demonstration of exceptional control, switching speed, and stability of the hidden state are key for device applications at the nexus of electronics and photonics.**

## INTRODUCTION

Controlling material properties on demand remains a long-standing challenge in condensed matter physics. Inspired by femtochemistry, the illumination by ultrashort light pulses poses a promising route to understanding and actively manipulating the macroscopic properties of quantum materials. Multiple optical control pathways have been established based on a transient modification of the free-energy landscape, ultrafast heating, and Floquet engineering (*1*). These control schemes allow, for example, triggering electronic phase transitions on femto- to picosecond timescales (*2*) and steering intricate structural transitions by excitation of specific lattice modes (*3*). In materials with multiple competing orders, ultrashort light pulses can also induce metastable states that feature properties inaccessible under thermodynamic equilibrium conditions, so-called hidden phases. As hidden phases expand emergent functionalities of complex solids, are often switchable on ultrafast timescales, and provide insights into fundamental interactions and phase competition, they are of high interest from a scientific and an application perspective. Prominent examples include optical switching to hidden metallic states in strongly correlated materials (*4*, *5*) and possible photoinduced superconductivity at temperatures far above the critical temperature $T_c$ (*6*). Yet, the microscopic processes governing the transition to metastable states often lack a clear understanding, resulting in unspecific empirical switching protocols with nonoptimal efficiencies and limited control over stability. Furthermore, most hidden phases persist only transiently on a picosecond timescale, precluding any practical application in switchable devices.

A particularly interesting metastable state is the metallic hidden (H) phase of 1*T*-$TaS_2$, as it can be reversibly induced by optical or electrical pulses and is accompanied by an insulator-to-metal transition with an orders-of-magnitude drop in resistivity (*7*–*15*). In addition, the H phase is exceptionally long-lived and thus represents a promising platform for device functionality (*16*). In equilibrium, the layered transition metal dichalcogenide 1*T*-$TaS_2$ features multiple competing ground states resulting from the interplay of Coulomb repulsion, Fermi surface nesting, and interlayer interaction. Of particular interest are several charge density wave (CDW) phases, which can be described by the formation of star-of-David (SOD) shaped clusters of ions that are inward radially displaced toward an unbound charge localized at the cluster centers (Fig. 1A). The SOD cluster formation gives rise to a metallic nearly commensurate (NC) CDW phase below 350 K that consists of patches of ordered clusters separated by smooth periodic domain walls (Fig. 1B). Cooling below 180 K leads to a hysteretic first-order transition to a commensurate (C) CDW phase with long-range intralayer order (Fig. 1C) (*17*), which is discussed to host a Mott-insulating state (*18*, *19*). In addition, in the C phase, an interlayer alignment of SOD clusters leads to a unit cell doubling along the out-of-plane direction, referred to as interlayer stacking order, which is suspected to strongly affect the low-energy electronic states (*9*, *19*–*22*).

Optical or electrical excitation of the C ground state triggers a transition to the metallic metastable H phase, which consists of microscopic commensurate domains intersected by a large number of irregular domain walls that induce an abrupt CDW phase slip between neighboring domains (Fig. 1D). While the atomic structure of the H phase has been studied extensively (*9*–*12*), the origin of the

[1]Fritz-Haber-Institut der Max-Planck-Gesellschaft, Faradayweg 4-6, D-14195 Berlin, Germany. [2]Department of Complex Matter, Jožef Stefan Institute, Jamova 39, SI-1000 Ljubljana, Slovenia. [3]Center of Excellence on Nanoscience and Nanotechnology – Nanocenter (CENN Nanocenter), Jamova 39, SI-1000 Ljubljana, Slovenia. [4]Stanford Institute for Materials and Energy Sciences, SLAC National Accelerator Laboratory, 2575 Sand Hill Road, Menlo Park, CA 94025, USA. [5]Geballe Laboratory for Advanced Materials, Departments of Physics and Applied Physics, Stanford University, Stanford, CA 94305, USA. [6]Institut für Optik und Atomare Physik, Technische Universität Berlin, Straße des 17. Juni 135, 10623 Berlin, Germany.
*Corresponding author. Email: rettig@fhi-berlin.mpg.de
†Present address: Department of Physics and Regensburg Center for Ultrafast Nanoscopy (RUN), University of Regensburg, Universitätsstrasse 31, 93053 Regensburg, Germany.
‡Present address: Université de Bordeaux - CNRS - CEA, CELIA, UMR5107, F33405 Talence, France.
§Present address: University of Chicago, Pritzker School of Molecular Engineering, Chicago, IL 60637, USA.
||Present address: Materials Science and Technology Division, Oak Ridge National Laboratory, Oak Ridge, TN 37831, USA.

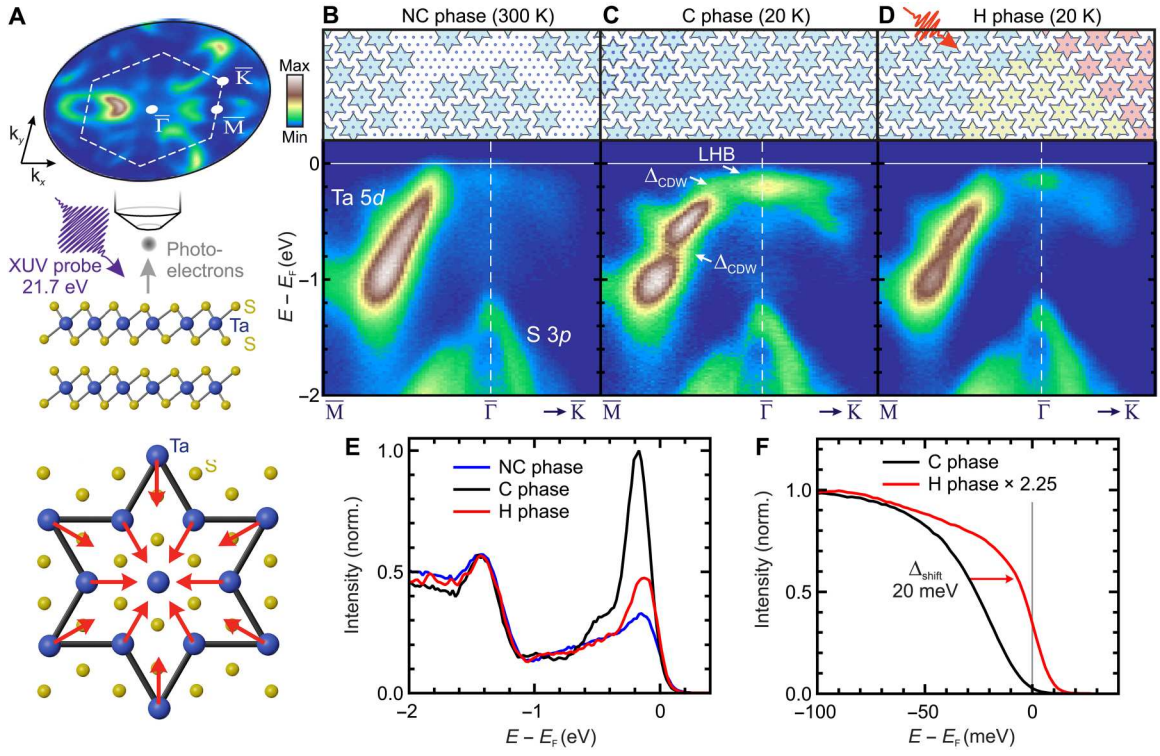


**Fig. 1. Band structure mapping.** (**A**) Top: Schematic of the static extreme ultraviolet (XUV) angle-resolved photoemission spectroscopy (ARPES) measurements and the layered 1*T*-$TaS_2$ sample. An exemplary isoenergy surface of the NC phase ($E - E_F = -0.5$ eV, momentum radius $k_{||} \sim 2$ Å$^{-1}$) with hexagonal surface Brillouin zone and high symmetry points is shown. Bottom: Illustration of the star-of-David (SOD) shaped cluster. (**B** to **D**) Top: Schematic intralayer order of the NC, C, and H phases (domains indicated by different colors). Bottom: ARPES energy-momentum cuts along the high-symmetry directions of the respective phases. Switching to the H phase was achieved by a single optical pulse at $h\nu = 1.55$ eV at an absorbed fluence $> F_{crit} \sim 0.5$ mJ cm$^{-2}$. (**E**) Energy distribution curves (EDCs) of the examined phases at $\bar{\Gamma}$. (**F**) EDCs of C and H phases at $\bar{\Gamma}$ near $E_F$ (gray line), obtained with a laser ARPES setup with high-energy resolution (see Materials and Methods).

metallization is still under debate (*7*, *10*, *12*, *19*) as measurements of the electronic band structure have been missing. Furthermore, although an electron-hole imbalance following the excitation has been suggested as a driver of the transition to the H state (*7*), a microscopic understanding of the switching mechanism—imperative for improving the switching energy and speed of memory devices based on metastable configurations (*16*)—has remained elusive. In particular, the role of coherences, which have been exploited to boost the switching efficiency in other systems (*3*), has remained largely unexplored.

Here, we use time- and angle-resolved photoemission spectroscopy (trARPES) to probe the electronic band structure and formation dynamics of the metastable H quantum state in bulk 1*T*-$TaS_2$ upon near-infrared femtosecond optical excitation. Using a combination of extreme ultraviolet (XUV) and ultraviolet (UV) trARPES, we map out the band structure of the H phase within the full first Brillouin zone and at high-energy resolution. We observe a global collapse of the Mott-insulating state, providing further hints for the critical role of the interlayer stacking order. Tracking the electron dynamics during the photoinduced phase transition from the C ground state to the H phase reveals an unexpectedly fast timescale of a few hundreds of femtoseconds, suggesting a highly efficient nonthermal switching pathway governed by a collective CDW excitation. Using a two-pump-pulse excitation scheme, we demonstrate vibrational coherent control of the transition to the H phase, evident from pump-pump-delay–dependent oscillations of the switching efficiency at the CDW amplitude mode (AM) frequency. On the basis of the observed band structure dynamics, we discuss an ultrafast microscopic switching pathway from C to H phase. Our study demonstrates exceptional control over the properties of complex solids by using tailored optical multi-pulse excitations of ordered states and highlights a promising route in the search for previously undiscovered hidden states.

## RESULTS

### Band structure mapping

First, we map out the static band structure along the high-symmetry directions for the different phases (Fig. 1). In the NC phase at room temperature, Ta 5*d* states give rise to a metallic low-energy band that reaches up to the Fermi level ($E_F$) at $\bar{\Gamma}$. Upon cooling, the gapped C phase emerges, as the SOD clusters become commensurate with the atomic lattice. This periodic charge and lattice distortion leads to a splitting of the Ta 5*d* band into subbands due to the formation of CDW energy gaps $\Delta_{CDW}$, with *d* electrons of the 12 outer Ta atoms of the star-shaped clusters occupying the subbands up to $E - E_F \sim -0.4$ eV. The remaining 13th electron remains localized on the central Ta atom due to strong on-site Coulomb repulsion, giving rise to a narrow and intense lower Hubbard band (LHB) at −0.2 eV and the opening of a small Mott gap at $E_F$, in agreement with

previous observations (*23*). Notably, switching from the C ground state to the persistent H phase at 20 K by a single optical pulse induces a marked modification of the low-energy states. Most notably, the LHB intensity is strongly suppressed, as evidenced by the energy distribution curves (EDCs) at $\overline{\Gamma}$ (Fig. 1E), accompanied by a suppression of the Mott gap (Fig. 1F and fig. S11). While, strictly speaking, the low-energy band in the H phase is a strongly-correlated metallic band (*22*), we refer to it as LHB across all phases.

Since ARPES is only sensitive to short-range order and averages over a macroscopic surface area due to the micrometer-sized probe beam, the marked spectral change upon switching from C to H phase is remarkable, as both phases consist predominantly of commensurately ordered SOD clusters, with only a fraction of the H phase consisting of domain walls (fig. S12). However, recent studies demonstrated a strong influence of the interlayer stacking order on the low-energy electronic states (*9*, *19*–*22*). As Ta $5d_{z^2}$ orbitals with strong out-of-plane character are located at the cluster centers, the interlayer orbital overlap is highly sensitive to the interlayer alignment. While, in the C ground state, two neighboring layers dimerize, switching to the H phase induces a multitude of irregular domain wall networks in each layer which shift the central cluster atoms by one or more atomic lattice vectors in different directions (*11*). These irregular phase shifts of the intralayer order within each layer induce disorder along the out-of-plane direction, breaking the long-range order of the interlayer dimerization (*12*) and thus reducing interlayer hopping. This external restacking may induce metallization, as the subtle balance of onsite Coulomb repulsion, and intra- and interlayer hopping is perturbed, quenching the fragile Mott state (*9*, *19*). Our measurements directly support this scenario, as we observe suppression of the LHB and closing of the Mott gap despite only minimal changes in the intralayer ordering. The metallization of a Mott insulator upon reducing interlayer hopping is consistent with a simple bilayer Hubbard model (*24*), although a more realistic theoretical treatment is required to capture the respective phases of $TaS_2$.

## Dynamical phase transition

Having established the spectral fingerprints of the H state, we next investigate the dynamical transition from C to H phase. Stroboscopic pump-probe trARPES measurements of the electronic switching dynamics (Fig. 2A) require relaxation to the C ground state between successive pump-probe cycles—not feasible at very low temperatures due to the exceptionally long lifetime of the H phase (*8*). Thus, we increase the sample temperature to 160 K, which reduces the lifetime to <100 μs and allows us to study the transition of the unperturbed C ground state to the H phase in a pump-probe experiment at a repetition rate of 10 kHz. We focus on the dynamics of the LHB at $\overline{\Gamma}$ for various pump-laser fluences ranging from the weak-response regime to above the switching threshold [see exemplary EDCs in Fig. 2 (B and C) and dispersion plots in fig. S13]. Using Gaussian fits of the EDCs (see Supplementary Text), we extract the dynamical evolution of the LHB peak intensity, the most discernible fingerprint to identify the H phase, as well as the transient shift of the LHB energy position.

For an absorbed fluence of 0.15 mJ $cm^{-2}$, far below the switching threshold, optical excitation launches a collective, coherent oscillation of the periodic charge and lattice distortion, termed amplitude mode, corresponding to an expansion-contraction motion of the SOD clusters (Fig. 2D) at 2.4 THz (*25*). Because of strong electron-phonon coupling, this causes a modulation of the LHB energy at the frequency of the AM (gray curve in Fig. 2E). While several bands across the full Brillouin zone are transiently renormalized by the CDW modulation, the energetic position of the LHB at $\overline{\Gamma}$ couples most strongly to the CDW and can thus be used as a measure of the CDW lattice displacement (*26*, *27*). In addition, within 50 fs after the excitation, the LHB intensity is reduced by ~40%, resulting from an initial quench of the Mott state by transient heating and depopulation of the LHB by electron-hole excitations into higher-lying states (*18*), followed by a full recovery within a few picoseconds (gray curve in Fig. 2F).

With increasing fluence, the initial band shift grows, while the AM oscillations become less pronounced, and the LHB intensity only partially recovers within the examined time range. Last, for the highest applied fluence of 0.7 mJ $cm^{-2}$, the system undergoes a transition from C to H phase, evidenced by a strong persistent quench of the LHB intensity that shows no onset of recovery within tens of picoseconds. Concomitantly, within 250 fs, the LHB undergoes a colossal transient metallization, shifting upward by ~300 meV, far above the equilibrium $E_F$, followed by a damped exponential recovery. This marked shift indicates a pronounced cooperative lattice motion counteracting the CDW distortion and, as the band shifts substantially above the band position of the metallic high-temperature phases (*28*), hints toward an overshoot of the displacement beyond the symmetric undistorted state, which has also been observed in the related compound 1*T*-$TaSe_2$ (*29*). The absence of AM modulations further supports the scenario of a strong disruption of the CDW order during the phase transition. Within ~800 fs, the LHB position relaxes to the new quasi-equilibrium position, and the transition is completed, in general agreement with switching times reported by optical studies (*13*–*15*).

Since the transition from C to H phase involves a major reorganization of the lattice, the observed switching time is unexpectedly short—far below the timescale of electron-lattice equilibration (*16*)—suggesting a highly efficient nonthermal collective transition pathway involving selective lattice modes. The question naturally arises of which mode facilitates such a coupled electronic and structural transition. The AM appears to be the most likely driver of such a concerted transition, as it connects electronic and structural orders and evolves, with increasing fluence, from an oscillatory motion into an unusually large band shift associated with a marked cooperative lattice response.

## Vibrational coherent control of the phase transition

To map out the role of the collective CDW excitation in the transition to the H phase, we perform trARPES measurements with two time-delayed optical pump pulses. The aim is to coherently control the AM (Fig. 3A). The initial pulse excites the AM, whereas the oscillation amplitude is either amplified (in-phase excitation) or suppressed (out-of-phase excitation) by the time-delayed second pulse (*3*, *30*, *31*). We first demonstrate coherent control of the AM in the C phase in the weak-response regime with both pump pulses at equal fluence far below $F_{crit}$ (see Supplementary Text). Using again the transient LHB position at $\overline{\Gamma}$ as a proxy of the CDW symmetry breaking, we observe, upon two-pulse excitation, a strong modulation of the AM oscillation amplitude as a function of pump-pump delay $t_{12}$ with the period of the AM—indicating effective coherent control.

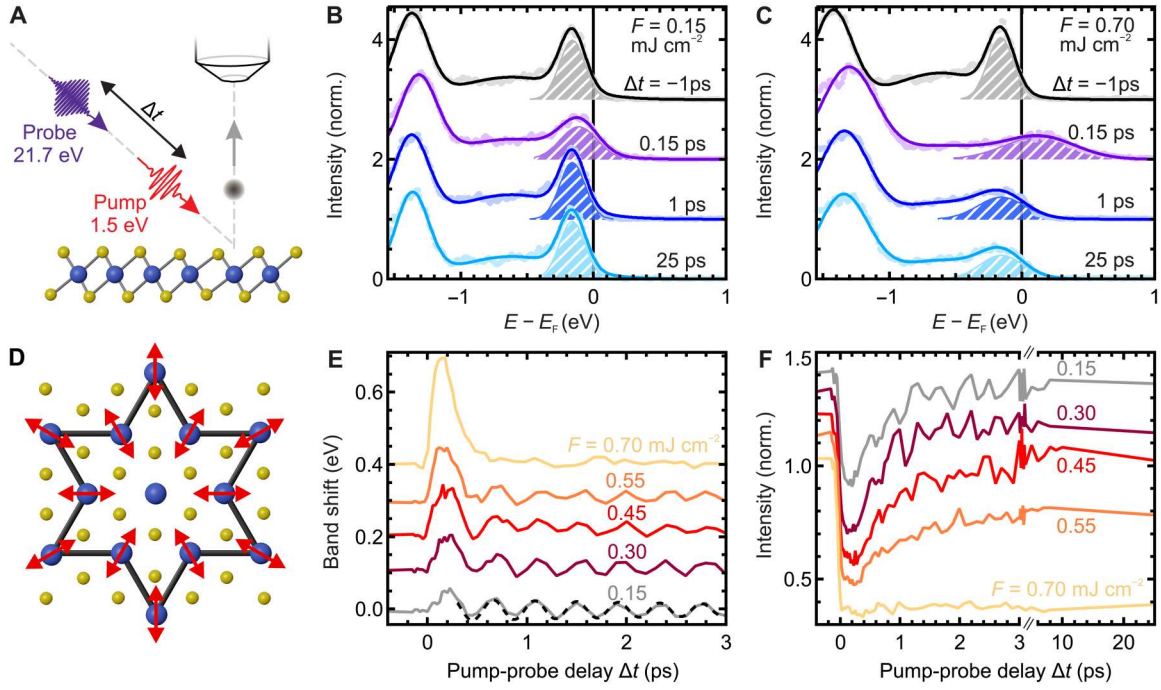


**Fig. 2. Dynamical transition to the H phase.** (**A**) Sketch of the trARPES experiment with pump-probe delay Δ*t*. (**B**) EDCs (dots) at $\bar{\Gamma}$ for selected delays after excitation at fluences below and (**C**) above the threshold fluence of the H phase ($T$ = 160 K, rep. rate = 10 kHz). The solid lines mark best fits using three Gaussian peaks as described in Supplementary Text. The shaded areas indicate the Gaussian peak capturing the LHB. For plots of the momentum-dependent evolution, see fig. S13. (**D**) Illustration of the collective oscillation of the star-shaped lattice distortion (CDW AM). (**E**) Band shift of the LHB versus Δ*t* for various fluences, extracted from the corresponding Gaussian center position. The dashed black line marks a sinusoidal fit ($f$ = 2.4 THz). (**F**) Peak intensity of the LHB versus Δ*t* for various fluences, extracted from the Gaussian fits. Curves are vertically offset for clarity.

Next, we increase the fluence to $F_1 = F_2 = 0.3$ mJ cm$^{-2}$, staying below the critical fluence of the H phase for each individual pulse, but crossing the threshold in combination. By monitoring the LHB at a fixed pump $_1$-probe delay of 35 ps, we probe the system after the new quasi-equilibrium is formed. Varying the pump-pump delay, we track whether the system has been switched to the H phase (strongly reduced LHB intensity) or remains in the C ground state (only minor reduction). Notably, the LHB intensity and position feature a pronounced modulation with pump-pump delay, as evinced by the strongly $t_{12}$-dependent EDCs at $\bar{\Gamma}$ (fig. S3). This dependence is highlighted by the phase transition efficiency, a parameterization of the $t_{12}$-dependent LHB intensity corresponding to the fraction of switched sample area (Fig. 3B). The coherent modulation of the switching efficiency with $t_{12}$ at 2.2(1) THz, corresponding to the AM frequency at 160 K (*7*, *25*) provides direct evidence for the decisive role of the collective CDW excitation in the photoinduced transition and demonstrates exceptional control over the phase transition using a multipulse excitation protocol. The distinct dependence of the switching efficiency rules out a temperature-driven transition from C to H phase, since, in a thermal switching scenario, the efficiency would only depend on the total deposited energy and would show no strong dependence on $t_{12}$ within the studied range. Note that the effect of absorption modulation by the AM as discussed, e.g., in (*3*) would be far too weak to explain our observations (see Supplementary Text).

Inspecting the phase of the switching efficiency reveals that its local maxima approximately coincide with the constructive amplification of the AM by the second optical pulse, while minima coincide with the suppression of the AM by the subsequent pulse (fig. S14). This indicates that, upon constructive amplification of the CDW excitation beyond a certain threshold, the transition to the H phase commences, while suppression impedes switching. Already at a fluence of 0.3 mJ cm$^{-2}$, a faint suppression of the LHB is observed by a single pulse, resulting in a switching efficiency of ~0.5 for two individual pulses with large pump-pump delay (gray line in Fig. 3B). Within the first oscillation cycle, coherent control of the AM allows suppressing the switching efficiency below the level of two individual pulses, demonstrating an effective suppression of the phase transition by the pulse sequence. Coherent amplification and suppression pathways within transient energy surfaces are sketched in Fig. 3 (C and D). Note that the one-dimensional (1D) energy landscape only serves as a schematic illustration. The offset of the local extrema of the switching efficiency from optimal amplification and suppression of the AM in the low-fluence regime by a few tens of femtoseconds suggests that the transition is governed by a more complex multidimensional energy landscape defined by intra- and interlayer CDW order (fig. S14).

## DISCUSSION

Our results demonstrate the ultrafast timescale and vibrational coherent control of the transition from C to H phase and expose the collective CDW excitation as an integral part of the optical switching mechanism. The colossal upward band shift of the LHB in the strong-response regime, the rapid transition within a few hundreds of femtoseconds, and the control of the switching efficiency

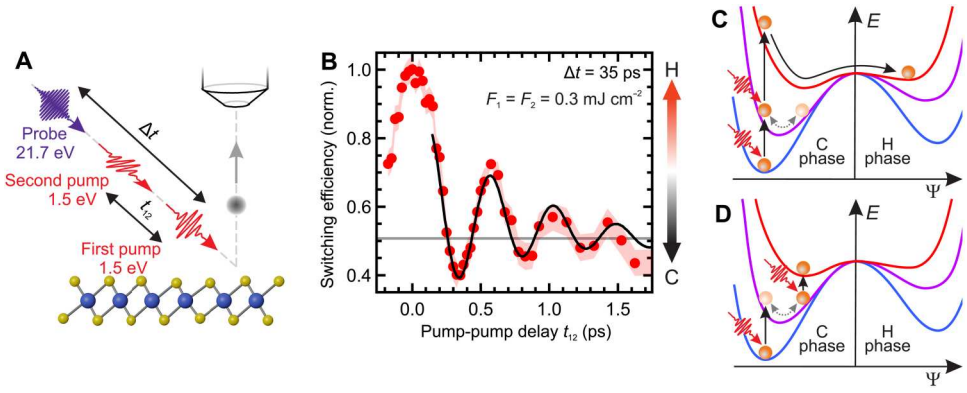


**Fig. 3. Coherent control of the transition to the H phase.** (**A**) Schematic of the trARPES experiment with two successive optical excitation pulses with pump-pump delay $t_{12}$ and pump-probe delay Δ*t*. To avoid interference artifacts during the cross-correlation, the pump pulses are linearly cross-polarized. (**B**) Switching efficiency (red dots) versus $t_{12}$, derived from the LHB intensity, with sinusoidal fit (black curve, $f = 2.2$ THz). An efficiency of 1 corresponds to the H phase, derived from the LHB intensity at $t_{12} = 0$ ps, while an efficiency of 0 corresponds to the LHB intensity of the unperturbed C ground state at 160 K (see Supplementary Text for details of the parameterization). The solid gray line indicates the asymptotic behavior for large pump-pump delays. The red shaded area indicates an uncertainty of one SD derived from the Gaussian fits. (**C**) Schematic energy surfaces in equilibrium (blue) and after excitation by a first (purple) and second (red) optical pulse. The system's order is parameterized by the order parameter Ψ along the AM coordinate. Depending on the pump-pump delay, the excitation leads to an efficient pathway to the H phase or (**D**) to a halt of the dynamics, suppressing the transition.

through the AM imply a nonthermal, cooperative transition pathway dictated by a transient energy landscape. Note that this behavior, as well as the ultrafast transition, the temperature-independent critical fluence, and the tens of microsecond-long lifetime of the transient state, excludes an incoherent thermal transition into a transient NC phase (see also Supplementary Text). On the basis of the observed band structure dynamics, we propose a microscopic pathway for the photoinduced phase transition (Fig. 4): Initially, the system is in the Mott-insulating C phase. The optical pump pulse is absorbed by the electronic system, which thermalizes within tens of femtoseconds, reaching a maximum temperature far beyond 1000 K (*7*, *26*) and melting the Mott energy gap (*18*). Simultaneously, the strong electronic perturbation displaces the ionic coordinates from their CDW ground-state positions toward the high-temperature symmetric positions, launching a delayed outward motion toward these new quasi-equilibrium coordinates. Concomitantly, the commensurate CDW energy gaps close, and the LHB is renormalized toward higher energies. Strong optical perturbation can lead to an overshoot of the ionic displacement beyond the undistorted high-symmetry positions. While for most CDW materials such an overshoot leads to a CDW pattern that is geometrically equivalent to the initial CDW (*32*, *33*), overdriving the SOD-shaped clusters leads to the formation of a new (inverted) CDW geometry. In the compound 1*T*-$TaSe_2$, which features a similar star-shaped CDW, the formation of an inverted CDW state—shifting the lattice and charge density from the cluster center to the

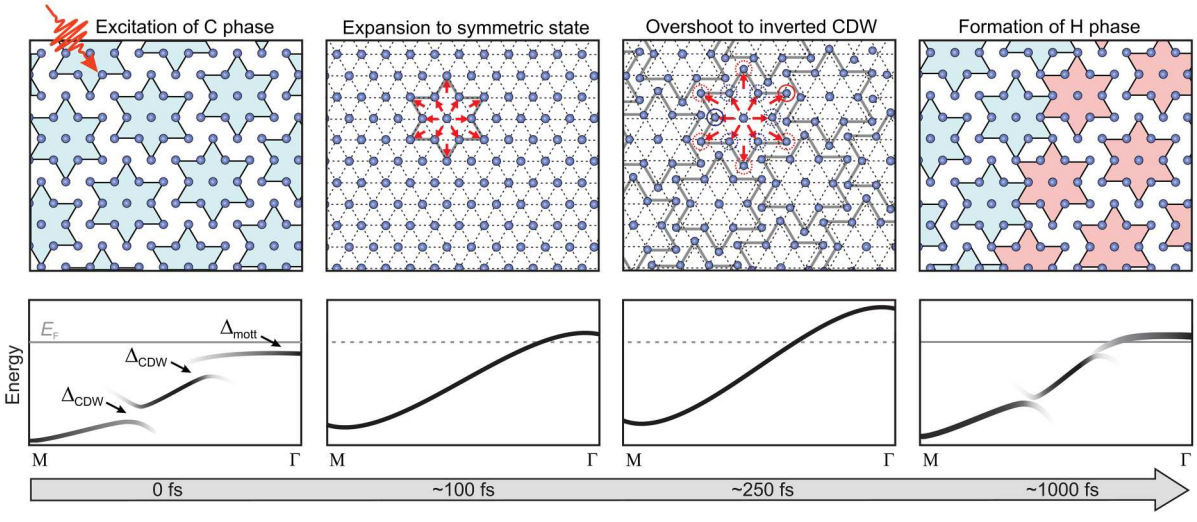


**Fig. 4. Illustration of the transition to the H state.** Top: Illustration of the intralayer lattice structure during the phase transition from C to H phase following a collective CDW excitation (see text). Red and blue circles indicate possible positions for the reformation of SOD clusters. Bottom: Corresponding schematic dispersion of the Ta 5*d* band. The gray horizontal line marks the equilibrium $E_F$. In the highly out-of-equilibrium state after photoexcitation, the position of $E_F$ is not well defined, as indicated by the dashed line.

peripheral—was observed, associated with a pronounced upward shift of the low-energy band at $\overline{\Gamma}$ (*29*). Similarly in $TaS_2$, the observed colossal shift of the LHB position within 250 fs suggests a CDW overshoot to an inverted pattern. Subsequently, on a timescale of a few hundreds of femtoseconds, the LHB position relaxes, which we assign to the reemergence of SOD clusters. However, because of strong damping in the transient metallic state, new SOD clusters nucleate around positions in the SOD peripheral, where atoms are closest in the inverted SOD pattern (circles in Fig. 4). As there are various equivalent positions for this reformation, the system is highly frustrated and forms a network of irregular domain boundaries in each $TaS_2$ layer. This leads to persistent breaking of the interlayer stacking order and quenching of the delicate Mott gap of the C phase, observed by the sustained collapse of the Mott-insulating state in the H phase. For an animation of an exemplary pathway, see movie S1. Note that similar suppression of interlayer correlations has recently also been shown in photoexcited $TaS_2$ and 1*T*-$TiSe_2$ using ultrafast electron diffraction (*34*, *35*).

The question arises as to whether the formation of the H phase plays out through an incoherent formation process or a collective pathway connected to the inverted CDW pattern. The ultrafast switching time suggests the latter, likely facilitated by the strong coupling of the overdriven CDW state to other vibrational modes (*36*, *37*) that enable efficient reformation of SOD clusters. As the CDW order in 1*T*-$TaS_2$ is rotated by ~13° with respect to the atomic lattice, previous studies showed that optical excitation of the room-temperature NC phase, which transiently completely suppresses the NC order, leads to the reformation of the NC phase in patches of two degenerate (clockwise and counterclockwise rotated) CDW domains (*38*). However, in the H phase, only a single rotational orientation similar to the initial CDW rotation in the C phase is observed (*11*), suggesting that a nonthermal transition pathway, which preserves the orientation, connects the C and H phases. Yet, the large number of irregular domain walls also indicates a high degree of disorder during the recovery. Within our coherent model, this disorder is introduced by the frustration of the transient anti-SOD pattern. As a previous explanation, an effective charge injection by photoexcitation has been proposed (*7*, *16*). In agreement with our description, the additional charges are accommodated in domain walls within the commensurate structure during the recovery of order, effectively increasing the electron density as neighboring stars within the domain walls share corners (*11*). Local fluctuations and aggregation of excess charges may thus interplay with a cooperative recovery of CDW order, resulting in the formation of the H phase. Additional studies of the ultrafast lattice dynamics are required to elucidate the microscopic details during the reformation of short-range CDW order.

The H phase can also be induced by optical or voltage pulses with pulse lengths that substantially exceed the period of the AM (*7*, *16*), precluding any collective CDW response. However, switching by an incoherent charge-carrier injection by optical picosecond pulses requires substantially higher switching energy densities (*7*). This demonstrates that, while the H phase can also be stabilized by an incoherent excitation, the collective switching pathway enables a more rapid and efficient transition.

In conclusion, using trARPES, we provide a detailed characterization of the electronic band structure and switching dynamics of the metastable hidden state of 1*T*-$TaS_2$ upon femtosecond optical excitation, thereby revealing the key role of a collective charge-density-wave excitation in the nonthermal transition pathway. The exceptional speed and high degree of control over the phase transition in combination with the remarkable stability of the hidden phase underline its unique functionality for memory devices (*16*) or optoelectronic applications. Furthermore, we envision that collective excitations of complex symmetry-broken ground states may reveal hidden orders in a variety of materials (*39*). In particular, resonant (multipulse) excitations of coherences, minimizing detrimental heating of the electrons and lattice, represent a promising route to realizing and understanding new emergent phases in quantum materials.

## MATERIALS AND METHODS

### XUV trARPES

Crystals of 1*T*-$TaS_2$ were grown by chemical transport method with iodine as a transport agent. The ARPES measurements were performed in ultrahigh vacuum $<1 \times 10^{-10}$ mbar (samples cleaved in situ), using a table-top high-harmonic-generation trARPES setup (*40*, *41*) ($h\nu_{probe}$ = 21.7 eV, $h\nu_{pump}$ = 1.55 eV, $\Delta E \approx 150$ meV, $\Delta t \approx 35$ fs) with a pulse picker to vary the repetition rate (from single pulses up to 500 kHz). The samples are positioned with a six-axis manipulator with cryogenic temperature control (SPECS Carving). Photoelectrons are collected either by a SPECS Phoibos 150 hemispherical analyzer or a SPECS METIS 1000 time-of-flight momentum microscope. The momentum microscope allows parallel acquisition of the 3D photoelectron distribution across a large energy and in-plane momentum range, advantageous for static band structure mapping (Fig. 1, A to E; and figs. S4; S5, C and D; S6, top; S7; and S8), while the hemispherical analyzer allows for fast data acquisition of 2D energy-momentum cuts, ideal for time-resolved measurements within a limited energy-momentum range at low repetition rates (Figs. 2 and 3 and figs. S1; S2; S3; S5, A and B; S6, bottom; S13; and S14).

The EDCs extracted from momentum microscopy data were integrated over a momentum area of $0.2 \times 0.2$ Å$^{-2}$. The EDCs extracted from hemispherical-analyzer data were integrated along the momentum-resolved direction over 0.35 Å$^{-1}$. For the applied probe energy of 21.7 eV, an inner potential $V_0$ = 20 eV and work function $\Psi$ = 4.5 eV of 1*T*-$TaS_2$ (*42*), we estimate that, within the 3D Brillouin zone, we map the band structure approximately at the Brillouin zone center with respect to the out-of-plane $k_z$ direction.

The pump and probe spot sizes (full width at half maximum, FWHM) are $\approx 150 \times 150$ μm$^2$ and $\approx 70 \times 60$ μm$^2$, respectively. All discussed fluences refer to the absorbed fluence, estimated using a complex refractive index of $n$ = 3.2 and $k$ = 2.9 at $\lambda$ = 800 nm. Temporal pump-probe overlap ($\Delta t$ = 0 fs) was determined from the transient pump laser–induced population of high-energy states ($E > E_F$ + 0.5 eV).

Switching to the H phase has been achieved using optical pulses at 800 nm and an absorbed fluence $>F_{crit} \approx 0.5$ mJ cm$^{-2}$ at a pulse length of $t_{FWHM}$ = 35 fs.

### UV trARPES

Additional static measurements (Fig. 1F and fig. S11) with increased energy resolution ($\Delta E < 22$ meV) were obtained using a 6-eV laser ARPES setup with a Scienta R4000 hemispherical analyzer (*43*). For

the 6-eV laser ARPES experiments, we used a regenerative amplifier operating at 10 kHz to switch the sample with 10-ms-long bursts consisting of 100 p-polarized 830-nm pulses at an absorbed fluence of 1 mJ $cm^{-2}$. The pump beam profile (FWHM) was 363 × 390 $\mu m^2$. The 6-eV laser ARPES was acquired with the frequency-quadrupled output of an oscillator operating at an 80-MHz repetition rate. The probe beam profile (FWHM) was 41 × 35 $\mu m^2$. During the 6-eV ARPES experiments, the sample was kept at 11 K.

## Supplementary Materials

**This PDF file includes:**
Supplementary Text
Figs. S1 to S14
Legend for movie S1
References

**Other Supplementary Material for this manuscript includes the following:**
Movie S1

## REFERENCES AND NOTES


1. A. de la Torre, D. M. Kennes, M. Claassen, S. Gerber, J. W. Mc Iver, M. A. Sentef, Colloquium: Nonthermal pathways to ultrafast control in quantum materials. *Rev. Mod. Phys.* **93**, 041002 (2021).
2. C. L. Smallwood, J. P. Hinton, C. Jozwiak, W. Zhang, J. D. Koralek, H. Eisaki, D.-H. Lee, J. Orenstein, A. Lanzara, Tracking cooper pairs in a cuprate superconductor by ultrafast angle-resolved photoemission. *Science* **336**, 1137–1139 (2012).
3. J. G. Horstmann, H. Böckmann, B. Wit, F. Kurtz, G. Storeck, C. Ropers, Coherent control of a surface structural phase transition. *Nature* **583**, 232–236 (2020).
4. V. R. Morrison, R. P. Chatelain, K. L. Tiwari, A. Hendaoui, A. Bruhács, M. Chaker, B. J. Siwick, A photoinduced metal-like phase of monoclinic $VO_2$ revealed by ultrafast electron diffraction. *Science* **346**, 445–448 (2014).
5. J. Zhang, X. Tan, M. Liu, S. W. Teitelbaum, K. W. Post, F. Jin, K. A. Nelson, D. N. Basov, W. Wu, R. D. Averitt, Cooperative photoinduced metastable phase control in strained manganite films. *Nat. Mater.* **15**, 956–960 (2016).
6. M. Budden, T. Gebert, M. Buzzi, G. Jotzu, E. Wang, T. Matsuyama, G. Meier, Y. Laplace, D. Pontiroli, M. Riccò, F. Schlawin, D. Jaksch, A. Cavalleri, Evidence for metastable photo-induced superconductivity in $K_3C_{60}$. *Nat. Phys.* **17**, 611–618 (2021).
7. L. Stojchevska, I. Vaskivskyi, T. Mertelj, P. Kusar, D. Svetin, S. Brazovskii, D. Mihailovic, Ultrafast switching to a stable hidden quantum state in an electronic crystal. *Science* **344**, 177–180 (2014).
8. I. Vaskivskyi, J. Gospodaric, S. Brazovskii, D. Svetin, P. Sutar, E. Goreshnik, I. A. Mihailovic, T. Mertelj, D. Mihailovic, Controlling the metal-to-insulator relaxation of the metastable hidden quantum state in 1*T*-$TaS_2$. *Sci. Adv.* **1**, e1500168 (2015).
9. L. Ma, C. Ye, Y. Yu, X. F. Lu, X. Niu, S. Kim, D. Feng, D. Tománek, Y.-W. Son, X. H. Chen, Y. Zhang, A metallic mosaic phase and the origin of Mott-insulating state in 1*T*-$TaS_2$. *Nat. Commun.* **7**, 10956 (2016).
10. D. Cho, S. Cheon, K.-S. Kim, S.-H. Lee, Y.-H. Cho, S.-W. Cheong, H. W. Yeom, Nanoscale manipulation of the Mott insulating state coupled to charge order in 1*T*-$TaS_2$. *Nat. Commun.* **7**, 10453 (2016).
11. Y. A. Gerasimenko, P. Karpov, I. Vaskivskyi, S. Brazovskii, D. Mihailovic, Intertwined chiral charge orders and topological stabilization of the light-induced state of a prototypical transition metal dichalcogenide. *NPJ Quantum Mater.* **4**, 32 (2019).
12. Q. Stahl, M. Kusch, F. Heinsch, G. Garbarino, N. Kretzschmar, K. Hanff, K. Rossnagel, J. Geck, T. Ritschel, Collapse of layer dimerization in the photo-induced hidden state of 1*T*-$TaS_2$. *Nat. Commun.* **11**, 1247 (2020).
13. J. Ravnik, M. Diego, Y. Gerasimenko, Y. Vaskivskyi, I. Vaskivskyi, T. Mertelj, J. Vodeb, D. Mihailovic, A time-domain phase diagram of metastable states in a charge ordered quantum material. *Nat. Commun.* **12**, 2323 (2021).
14. J. Ravnik, I. Vaskivskyi, T. Mertelj, D. Mihailovic, Real-time observation of the coherent transition to a metastable emergent state in 1T–$TaS_2$. *Phys. Rev. B* **97**, 075304 (2018).
15. F. Y. Gao, Z. Zhang, Z. Sun, L. Ye, Y.-H. Cheng, Z.-J. Liu, J. G. Checkelsky, E. Baldini, K. A. Nelson, Snapshots of a light-induced metastable hidden phase driven by the collapse of charge order. *Sci. Adv.* **8**, eabp9076 (2022).
16. D. Mihailovic, D. Svetin, I. Vaskivskyi, R. Venturini, B. Lipovšek, A. Mraz, Ultrafast non-thermal and thermal switching in charge configuration memory devices based on 1*T*-$TaS_2$. *Appl. Phys. Lett.* **119**, 013106 (2021).
17. R. E. Thomson, B. Burk, A. Zettl, J. Clarke, Scanning tunneling microscopy of the charge-density-wave structure in 1*T*-$TaS_2$. *Phys. Rev. B. Condens. Matter* **49**, 16899–16916 (1994).
18. M. Ligges, I. Avigo, D. Golež, H. U. R. Strand, Y. Beyazit, K. Hanff, F. Diekmann, L. Stojchevska, M. Kalläne, P. Zhou, K. Rossnagel, M. Eckstein, P. Werner, U. Bovensiepen, Ultrafast doublon dynamics in photoexcited 1*T*-$TaS_2$. *Phys. Rev. Lett.* **120**, 166401 (2018).
19. C. J. Butler, M. Yoshida, T. Hanaguri, Y. Iwasa, Mottness versus unit-cell doubling as the driver of the insulating state in 1*T*-$TaS_2$. *Nat. Commun.* **11**, 2477 (2020).
20. T. Ritschel, J. Trinckauf, K. Koepernik, B. Büchner, M. V. Zimmermann, H. Berger, Y. I. Joe, P. Abbamonte, J. Geck, Orbital textures and charge density waves in transition metal dichalcogenides. *Nat. Phys.* **11**, 328–331 (2015).
21. S.-H. Lee, J. S. Goh, D. Cho, Origin of the insulating phase and first-order metal-insulator transition in 1T–$TaS_2$. *Phys. Rev. Lett.* **122**, 106404 (2019).
22. C. W. Nicholson, F. Petocchi, B. Salzmann, C. Witteveen, M. Rumo, G. Kremer, Fabian O. von Rohr, P. Werner, C. Monney, Modified interlayer stacking and insulator to correlated-metal transition driven by uniaxial strain in 1T-TaS2. arXiv:2204.05598 (2022).
23. L. Perfetti, T. A. Gloor, F. Mila, H. Berger, M. Grioni, Unexpected periodicity in the quasi-two-dimensional mott insulator 1T–$TaS_2$ revealed by angle-resolved photoemission. *Phys. Rev. B.* **71**, 153101 (2005).
24. A. Fuhrmann, D. Heilmann, H. Monien, From mott insulator to band insulator: A dynamical mean-field theory study. *Phys. Rev. B* **73**, 245118 (2006).
25. J. Demsar, L. Forró, H. Berger, D. Mihailovic, Femtosecond snapshots of gap-forming charge-density-wave correlations in quasi-two-dimensional dichalcogenides 1T-$TaS_2$ and 2H-$TaSe_2$. *Phys. Rev. B* **66**, 041101 (2002).
26. L. Perfetti, P. A. Loukakos, M. Lisowski, U. Bovensiepen, H. Berger, S. Biermann, P. S. Cornaglia, A. Georges, M. Wolf, Time evolution of the electronic structure of 1T-$TaS_2$ through the insulator-metal transition. *Phys. Rev. Lett.* **97**, 067402 (2006).
27. S. Hellmann, T. Rohwer, M. Kalläne, K. Hanff, C. Sohrt, A. Stange, A. Carr, M. M. Murnane, H. C. Kapteyn, L. Kipp, M. Bauer, K. Rossnagel, Time-domain classification of charge-density-wave insulators. *Nat. Commun.* **3**, 1069 (2012).
28. C. Sohrt, A. Stange, M. Bauer, K. Rossnagel, How fast can a peierls–mott insulator be melted? *Faraday Discuss.* **171**, 243–257 (2014).
29. Y. Zhang, X. Shi, M. Guan, W. You, Y. Zhong, T. R. Kafle, Y. Huang, H. Ding, M. Bauer, K. Rossnagel, S. Meng, H. C. Kapteyn, M. M. Murnane, Creation of a novel inverted charge density wave state. *Struct. Dyn.* **9**, 014501 (2022).
30. D. Mihailovic, D. Dvorsek, V. V. Kabanov, J. Demsar, L. Forró, H. Berger, Femtosecond data storage, processing, and search using collective excitations of a macroscopic quantum state. *Appl. Phys. Lett.* **80**, 871–873 (2002).
31. L. Rettig, J.-H. Chu, I. R. Fisher, U. Bovensiepen, M. Wolf, Coherent dynamics of the charge density wave gap in tritellurides. *Faraday Discuss.* **171**, 299–310 (2014).
32. T. Huber, S. O. Mariager, A. Ferrer, H. Schäfer, J. A. Johnson, S. Grübel, A. Lübcke, L. Huber, T. Kubacka, C. Dornes, C. Laulhe, S. Ravy, G. Ingold, P. Beaud, J. Demsar, S. L. Johnson, Coherent structural dynamics of a prototypical charge-density-wave-to-metal transition. *Phys. Rev. Lett.* **113**, 026401 (2014).
33. J. Maklar, Y. W. Windsor, C. W. Nicholson, M. Puppin, P. Walmsley, V. Esposito, M. Porer, J. Rittmann, D. Leuenberger, M. Kubli, M. Savoini, E. Abreu, S. L. Johnson, P. Beaud, G. Ingold, U. Staub, I. R. Fisher, R. Ernstorfer, M. Wolf, L. Rettig, Nonequilibrium charge-density-wave order beyond the thermal limit. *Nat. Commun.* **12**, 2499 (2021).
34. T. Domröse, T. Danz, S. F. Schaible, K. Rossnagel, S. V. Yalunin, C. Ropers, Light-induced hexatic state in a layered quantum material. *Nat. Mater.* 10.1038/s41563-023-01600-6, (2023).
35. Y. Cheng, A. Zong, J. Li, W. Xia, S. Duan, W. Zhao, Y. Li, F. Qi, J. Wu, L. Zhao, P. Zhu, X. Zou, T. Jiang, Y. Guo, L. Yang, D. Qian, W. Zhang, A. Kogar, M. W. Zuerch, D. Xiang, J. Zhang, Light-induced dimension crossover dictated by excitonic correlations. *Nat. Commun.* **13**, 963 (2022).
36. E. S. Zijlstra, L. L. Tatarinova, M. E. Garcia, Laser-induced phonon-phonon interactions in bismuth. *Phys. Rev. B* **74**, 220301 (2006).
37. G. Sciaini, M. Harb, S. G. Kruglik, T. Payer, C. T. Hebeisen, F. J. z. Heringdorf, M. Yamaguchi, M. H.-V. Hoegen, R. Ernstorfer, R. J. D. Miller, Electronic acceleration of atomic motions and disordering in bismuth. *Nature* **458**, 56–59 (2009).
38. A. Zong, X. Shen, A. Kogar, L. Ye, C. Marks, D. Chowdhury, T. Rohwer, B. Freelon, S. Weathersby, R. Li, J. Yang, J. Checkelsky, X. Wang, N. Gedik, Ultrafast manipulation of mirror domain walls in a charge density wave. *Sci. Adv.* **4**, eaau5501 (2018).
39. N. Yoshikawa, H. Suganuma, H. Matsuoka, Y. Tanaka, P. Hemme, M. Cazayous, Y. Gallais, M. Nakano, Y. Iwasa, R. Shimano, Ultrafast switching to an insulating-like metastable state by amplitudon excitation of a charge density wave. *Nat. Phys.* **17**, 909–914 (2021).

40. M. Puppin, Y. Deng, C. W. Nicholson, J. Feldl, N. B. M. Schröter, H. Vita, P. S. Kirchmann, C. Monney, L. Rettig, M. Wolf, R. Ernstorfer, Time- and angle-resolved photoemission spectroscopy of solids in the extreme ultraviolet at 500 kHz repetition rate. *Rev. Sci. Instrum.* **90**, 023104 (2019).
41. J. Maklar, S. Dong, S. Beaulieu, T. Pincelli, M. Dendzik, Y. W. Windsor, R. P. Xian, M. Wolf, R. Ernstorfer, L. Rettig, A quantitative comparison of time-of-flight momentum microscopes and hemispherical analyzers for time- and angle-resolved photoemission spectroscopy experiments. *Rev. Sci. Instrum.* **91**, 123112 (2020).
42. A. S. Ngankeu, S. K. Mahatha, K. Guilloy, M. Bianchi, C. E. Sanders, K. Hanff, K. Rossnagel, J. A. Miwa, C. B. Nielsen, M. Bremholm, P. Hofmann, Quasi-one-dimensional metallic band dispersion in the commensurate charge density wave of *1T*-$TaS_2$. *Phys. Rev. B.* **96**, 195147 (2017).
43. A. Gauthier, J. A. Sobota, N. Gauthier, K.-J. Xu, H. Pfau, C. R. Rotundu, Z.-X. Shen, P. S. Kirchmann, Tuning time and energy resolution in time-resolved photoemission spectroscopy with nonlinear crystals. *J. Appl. Phys.* **128**, 093101 (2020).
44. S. Hellmann, C. Sohrt, M. Beye, T. Rohwer, F. Sorgenfrei, M. Marczynski-Bühlow, M. Kalläne, H. Redlin, F. Hennies, M. Bauer, A. Föhlisch, L. Kipp, W. Wurth, K. Rossnagel, Time-resolved x-ray photoelectron spectroscopy at FLASH. *New J. Phys.* **14**, 013062 (2012).
45. L.-P. Oloff, K. Hanff, A. Stange, G. Rohde, F. Diekmann, M. Bauer, K. Rossnagel, Pump laser-induced space-charge effects in HHG-driven time- and angle-resolved photoelectron spectroscopy. *J. Appl. Phys.* **119**, 225106 (2016).
46. Y. D. Wang, W. L. Yao, Z. M. Xin, T. T. Han, Z. G. Wang, L. Chen, C. Cai, Y. Li, Y. Zhang, Band insulator to Mott insulator transition in 1*T*-$TaS_2$. *Nat. Commun.* **11**, 4215 (2020).

**Acknowledgments:** We thank P. Sutar (Jožef Stefan Institute) for providing the samples. We thank T. Ritschel (Technische Universität Dresden), M. A. Sentef, D. B. Shin (MPI for the Structure and Dynamics of Matter), M. Müller, and L. Jiajun (Paul Scherrer Institut) for enlightening discussions. **Funding:** This work was funded by the Max Planck Society, the European Research Council (ERC) under the European Union's Horizon 2020 research and innovation program (grant no. ERC-2015-CoG-682843 and OPTOlogic 899794), the German Research Foundation (DFG) under the Emmy Noether program (grant no. RE 3977/1), the SFB/TRR 227 Ultrafast Spin Dynamics (projects A09 and B07, project-ID 328545488), the priority program SPP2244 (project-ID 443366970), and the DFG research unit FOR 1700. T.P. acknowledges financial support from the Alexander von Humboldt Foundation. The work by P.S.K., J.A.S., S.Y., D.L., R.G.M., and Z.-X.S. at Stanford and SLAC was supported by the Department of Energy, Office of Basic Energy Sciences, Division of Materials Science and Engineering. D.L. acknowledges support from the Swiss National Science Foundation, under fellowship no. P300P2_151328. S.Y. acknowledges support from the Stanford Graduate Fellowship. **Author contributions:** L.R., D.M., and J.M. conceived the experiment. J.M., S.D., J.S., T.P., S.B., and L.R. carried out the XUV trARPES experiments. P.S.K., J.A.S., S.Y., D.L., and R.G.M. carried out the 6-eV laser ARPES experiments. Y. A.G. conducted and analyzed the STM experiments. J.M. analyzed the data with support from L. R. and J.S. J.M. wrote the manuscript with support from L.R., Y.A.G., and D.M. L.R., R.E., M.W., and Z.-X.S. provided the experimental infrastructure. All authors commented on the paper. **Competing interests:** The authors declare that they have no competing interests. **Data and materials availability:** All data needed to evaluate the conclusions in the paper are present in the paper and/or the Supplementary Materials. The corresponding raw data files are publicly available at the Zenodo data repository under DOI 10.5281/zenodo.8238530.

Submitted 27 April 2023
Accepted 24 October 2023
Published 24 November 2023
10.1126/sciadv.adi4661

ScienceAdvances

# Coherent light control of a metastable hidden state

Julian Maklar, Jit Sarkar, Shuo Dong, Yaroslav A. Gerasimenko, Tommaso Pincelli, Samuel Beaulieu, Patrick S. Kirchmann, Jonathan A. Sobota, Shuolong Yang, Dominik Leuenberger, Robert G. Moore, Zhi-Xun Shen, Martin Wolf, Dragan Mihailovic, Ralph Ernstorfer, and Laurenz Rettig

*Sci. Adv.* **9** (47), eadi4661. DOI: 10.1126/sciadv.adi4661